Article:

Cationic Mn^{2+}/H^+ exchange leading a slow solid-state transformation of a 2D porphyrinic network at ambient conditions

Eder Amayuelas, Arkaitz Fidalgo-Marijuan, Begoña Bazán, Miren Karmele Urtiaga, Gotzone Barandika, Luis Lezama, María Isabel Arriortua

Cationic Mn^{2+}/H$^+$ exchange leading a slow solid-state transformation of a 2D porphyrinic network at ambient conditions

Eder Amayuelas,[a] Arkaitz Fidalgo-Marijuan,[a] Begoña Bazán,*[a,b] Miren Karmele Urtiaga,[a] Gotzone Barandika,[b,c] Luis Lezama[b,c] and María Isabel Arriortua[a,b]

aDepartamento de Mineralogía y Petrología, Facultad de Ciencia y Tecnología, Universidad del País Vasco (UPV/EHU), Apdo 644, 48080 Bilbao, Spain.

Email: bego.bazan@ehu.eus; Fax: +34-946013500; Tel: +34-946012609, eder.amayuelas@ehu.eus, arkaitz.fidalgo@ehu.eus, karmele.urtiaga@ehu.eus, maribel.arriortua@ehu.eus

bBCMaterials Parque Tecnológico de Zamudio, Ibaizabal Bidea, Edificio 500–Planta 1, 48160, Derio, Spain.

cDepartamento de Química Inorgánica, Facultad de Ciencia y Tecnología, Universidad del País Vasco (UPV/EHU), Apdo 644, 48080 Bilbao, Spain.

Email: gotzone.barandika@ehu.eus, luis.lezama@ehu.eus

Abstract

Metalloporphyrins exhibit outstanding chemical, physical and biological properties in dissolution, however, it is a challenge to synthesize them as stable solid frameworks. Long-time stability is crucial for future applications of these materials, and we have detected a slow, solid-state transformation of a 2D Mn^{II}-porphyrin at RT. The remarkable point is that this transformation showed up as a result of Electronic Paramagnetic Resonance measurements. Otherwise, the evolution of the system could have remained undetected. Thus, 2D [Mn$_3$(TCPP)(H$_2$O)$_4$]·nD (**1**) (where TCPP is *meso*-tetra(4-carboxyphenyl)porphyrin and D is *the sovent*) has been synthesized hydrothermally, and characterised by means of X-ray diffraction (XRD), Thermogravimetry and X-ray thermodiffractometry (XRTD). This compound slowly transforms into [Mn(H$_4$TCPP)(H$_2$O)$_2$]·nD (**2**) according to the equilibrium [Mn$_3$(TCPP)]+4H$^+$ ↔ [Mn(H$_4$TCPP)]+2Mn^{2+}. The evolution of the system has been studied through analysis of the distortion (both of the coordination sphere and the tetrapyrrolic macrocycle) and Density Functional Theory (DFT) quantum mechanical calculations.

Keywords: coordination polymer, porphyrin, structural analysis, DFT, thermal analysis, solvothermal synthesis

1. Introduction

Porpyrins are multifunctional biomolecules of great importance in biological complexes playing essential biochemical, enzymatic, and photochemical functions based on the special properties of the tetrapyrrolic macrocycle.[1] Due to the ubiquitous biological functions of metalloporphyrins in nature (for example light-harvesting,

oxygen transportation and catalysis), building coordination architectures using porphyrinic ligands becomes exceedingly desirable in pursuance of mimicking their diverse biological functionalities.[2] Metalloporphyrins are remarkable precursors in supramolecular chemistry, giving rise to a variety of materials because of their unique chemical, physical and biological properties.[3] In the wide horizons of Metal–Organic Frameworks (MOFs),[4] metalloporphyrin frameworks arouse intensive research interest, although it still remains in their premature stage. Accordingly, studies about common process in synthesis and crystal transformations have their interest in this area.[5]

MOFs´ stability has been identified as one of the most studied topics in this field, due to its relationship with their use in several applications. In fact, adsorption of ambient humidity by highly porous networks has been observed to alter the adsorption results, even provoking the collapse of the network in some cases.[6] Long-time stability is required from efficient materials, but information about this aspect is not usually reported.

One of the hot-topics in solid-state chemistry are solid-state structural transformations[7] including coordination polymers either produced by light, heat, uptake or exchange, guest removal, expansion of coordination numbers, condensation, oxidation of metal centers or reactions between the ligands. These structural transformations normally provoke significant rearrangement of molecular components in the crystals as reported by M. Hedayetullah Mir et al.[8] All these features can be studied through the distortion affecting both the coordination sphere and the tetrapyrrolic macrocycle, and this has been also a part of our approach to the analysis of the transformation.

Taking into account the above mentioned aspects, this work was focused on the preparation of metalloporphyrin based solid coordination networks. Our synthesis strategy includes first transition metals (which are abundant, environmentally friendly and have a variety of oxidation states and coordination spheres), meso-tetra(4-carboxyphenyl)porphyrin (H_6TCPP) and the use of a secondary ligand like 1,2,4,5-benzenetetracarboxylic acid (bta) with the aim of increasing porosity.[9] This work intended to explore the Mn^{II}-TCPP-bta combination. However, as will explain below, the bta ligand results not to be coordinated to the metal ion. A search in the CSD (Cambridge Structural Database 2016/09/01) shows that, even if the number of TCPP-based crystal structures is high (183 deposited structures), the number of compounds with TCPP containing Mn is significantly low (14 deposited structures).

Thereby, the work herein presented consists of the synthesis and characterization of $[Mn_3(TCPP)(H_2O)_4]\cdot nD$ (**1**) (D= N,N´dimethylformamide (DMF) or EtOH), and its slow transformation at ambient conditions (20 °C, 1 atm) into $[Mn(H_4TCPP)(H_2O)_2]\cdot nD$ (**2**). In this sense, we have detected a transformation occurring in a 2D system based on a Mn^{II}-porphyrin. The slowness of the system evolution and the low amount of the resulting product (a new solid network) could have resulted in the transformation remained hidden. However, Electron Paramagnetic Resonance (EPR) measurements have allowed us to detect it. Both compounds have been structurally characterized by means of X-ray diffraction (XRD). Thermal stability has been studied by means of TG

and XRTD. DFT calculations and distortion analysis on the coordination sphere and on the tetrapyrrolic macrocycle have been also carried out.

2. Experimental Section

2.1. Materials and general methods

The IR spectra were collected on a JASCO FT/IR-6100 spectrometer at room temperature at the range of 4000-400 cm^{-1}, in KBr pellets (1% of the sample). C, H, N and O elemental analyses were measured using a Euro EA 3000 elemental analyzer. Thermogravimetric analyses were carried out using a NETZSCH STA 449F3 thermobalance. A crucible containing approximately 10 mg of sample was heated at 5 °C min^{-1} in the temperature range 30-600 °C. The thermal behaviour was also studied using X-ray thermodiffractometry. A Bruker D8 Advance Vantec diffractometer (Cu-Kα radiation) equipped with a variable-temperature stage (Anton Paar HTK2000) with a Pt sample holder was used in the experiments. The powder patterns were recorded in 2θ steps of 0.0333° in the 5-38° range, counting for 0.8 s per step and increasing the temperature at 15 °C·min^{-1} from room temperature to 600 °C. Electron paramagnetic resonance (EPR) spectra were measured with A Bruker ELEXSYS 500 spectrometer equipped with a super-high-Q resonator ER-4123-SHQ, operating at X band, was used to record the EPR polycrystalline spectra. The magnetic field was calibrated by a NMR probe and the frequency inside the cavity was determined with an integrated MW-frequency counter.

2.2. Synthesis of $[Mn_3(TCPP)(H_2O)_4] \cdot nD$ (**1**) and $[Mn(H_4TCPP)(H_2O)_2] \cdot nD$ (**2**).

All solvents and chemicals were used as received from reliable commercial sources. The non-metallated meso-tetra(4-carboxyphenyl)porphyrin, manganese(II) nitrate hydrate 99.99%, 1,2,4,5-benzenetetracarboxylic acid (bta) and the solvents N,N-dimethylformamide 99.8% (DMF) and ethanol 96% were purchased from Sigma-Aldrich Co.

meso-tetra(4-carboxyphenyl)porphyrin (7.9 mg, 0.01 mmol), manganese(II) nitrate hydrate 99.99% (17.6 mg, 0.1 mmol) and 1,2,4,5-benzenetetracarboxylic acid (25.2 mg, 0.1 mmol), as crystallization helper (crystals were not obtained without bta used in the synthesis), were dissolved in a mixture of DMF (3 mL) and ethanol (1 mL) in a small capped vial, sonicated to ensure homogeneity and heated to 100 °C for 72 h, yielding prismatic and brown crystals of compound **1**, washed thoroughly with ethanol and dried in air at room temperature. vmax/cm^{-1}: 3390, (C(sp2)H), 3070 (OH), 1700 (C=O). 1600−1400 (CC), 1320 (CO), 1300 (CN), 1000 (MnTCPP). (Figure S1, Supplementary Information†). For compound **2** we just had to let fresh synthesized crystals in mother liquid, at ambient conditions (20 °C, 1 atm). However color and shape of crystals don´t change what made difficult distinguish each compound to the naked eye and proportions of each compound.

2.3. Single-crystal X-ray diffraction

X-ray structure determinations for compounds **1** and **2** single-crystals with dimensions given in Table 3 were selected under polarizing microscope and mounted on MicroMounts™. Single-crystal X-ray diffraction data were collected at 100 K on an

Agilent Technologies SuperNova single source diffractometer with Cu-Kα radiation (λ=1.54184 Å). Data frames were processed (unit cell determination, intensity data integration, correction for Lorentz and polarization effects,[10] and analytical absorption correction) using the CrysAlis software package.[11] The structure of compounds **1** and **2** were solved in the monoclinic C2/m and the tetragonal P4/nbm space groups respectively (Table 1), with OLEX program,[12] which allowed us to obtain the position of metal atoms, as well as nitrogen, oxygen and some of the carbon atoms of the porphyrin. The refinement of the crystal structure was performed by full matrix least-squares based on F^2, using the SHELXL-97 program[13] obtaining the remaining carbon atoms. Anisotropic thermal parameters were used for all non-hydrogen atoms (Figure S2 and S3, Supplementary Information†). All the hydrogen atoms connected to the aromatic rings (C-H 0.95Å) were fixed geometrically, and were refined using a riding model with common isotropic displacements. Some distances were fixed using DFIX instruction, and EADP and ISOR for some anisotropic parameters. Due to the low crystallinity of the single crystals for compound **1** and **2** solvent molecules were disordered in the crystal and the resulting electron density was found to be non-interpretable. The solvent contribution to the structure factors was taken into account by back-Fourier transformation of all the densities found in the disordered area using a solvent mask in OLEX.[12] The calculated density does not take into account the solvent causing disagreement between calculated and experimental density. Some hydrogen atoms of the carboxylic groups and ethanol molecules for compound **2** were not considered due to the lack of density in the residual density map; however they are included in the formula. Besides, several measurements were tried with the aim of improving completeness and diffraction data for compound **1**, with no success. Crystallographic data for the structures reported in this paper have been deposited in the Cambridge Crystallographic Data Center with CCDC 1046843–1449424 for **1**–**2**, respectively.

Table 1. Crystallographic data of compounds **1** and **2**

Compound	1	2
structural formula	$[Mn_3(TCPP)(H_2O)_4]\cdot nD$	$[Mn(H_4TCPP)(H_2O)_2]\cdot nD$
empirical formula	$C_{48}H_{24}Mn_3N_4O_{13}$	$C_{50}H_{26}MnN_4O_{12}$
Fw, g mol^{-1}	1029.54	931.7
Cryst. system	Monoclinic	Tetragonal
space group	C2/m	P4/nbm
a, Å	19.6713(16)	22.3162(4)
b, Å	23.7434(19)	
c, Å	9.9624(7)	12.0121(3)
α, deg		
β, deg	106.842(7)	
γ, deg		
V, Å^3	4453.5(6)	5977.7(2)
Z	2	4
ρobs, ρcal, g·cm^{-3}	1.346(5), 0.7677*	1.285(3), 1.035*
Crystal size, mm	0.16x0.08x0.05	0.19x0.13x0.09
μ, mm^{-1}	3.717	2.239

absorption correction	Analytical	Analytical
radiation, λ, Å	1.54184	1.54184
temperature, K	100.0(2)	100.0(2)
reflns collected, unique	6023, 2407 (Rint= 0.034)	46592, 1919 (Rint=0.062)
final R indices [I>2σ(I)]	R1 = 0.0798, wR2 = 0.1008	R1 = 0.0864, wR2 = 0.1129
R indices (all data)	R1 = 0.2677, wR2 = 0.2458	R1 = 0.3017, wR2 = 0.2748
GOF on F^2	1.0002	1.099
parameters/restraints	183/25	158/0

*Differences between observed and calculated density due to the squeeze tool in the structure refinement

3. Results and discussion

3.1. Crystal structures

The crystal structure of compound **1** arrays in layers. There are two crystallographically independent Mn atoms. One of them is located in the centre of the tetrapyrrolic units (Mn2), octahedrally coordinated to four N atoms that are coplanar. The axial positions are occupied by two O atoms that belong to water molecules. These metalloporphyrin units are linked by paddle-wheels consisting of two pentacoordinated manganese atoms (Mn1 and Mn1[i], i=−x+1, y, −z) coordinated to four oxygen atoms, corresponding to the carboxylate groups of TCPP, on the base of the square pyramid and to an axial oxygen atom of a water molecule. As shown in Figure 1, this arrangement gives rise to a 2D framework which grows just through the peripheral meso substituents of the porphyrin. Thus, each porphyrin is surrounded by other four, exhibiting cavities of 12 Å x 12 Å. Those voids are occupied by DMF and ethanol solvent molecules. Unfortunately we have not been able to localize them on the electronic density map during crystal structure refinement. These layers are stacked along the [10-1] direction, giving rise to a 3D supramolecular array. Even if the solvent molecules have not been localized, they are supposed to form hydrogen bonds between layers providing stability to the 3D array.
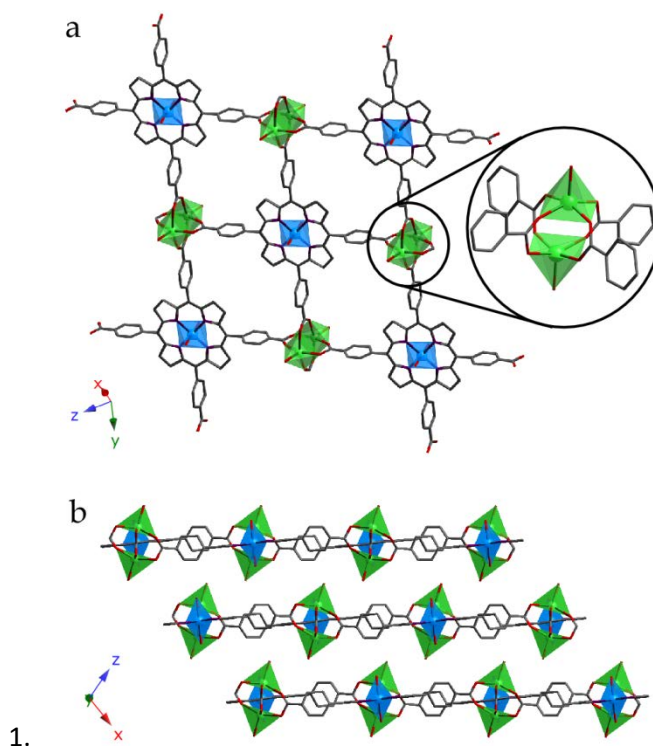
Figure 1. (a) 2D layer and a single paddle-wheel detail and (b) projection of the supramolecular arrangement for compound **1**. (Mn (porphyrin): blue, Mn (paddle-wheel): green, C: grey, N: dark blue, O: red). H atoms have been omitted for clarity.

The crystal structure of compound **2** shows that MnTCPP monomers arrange in supramolecular 2D layers which are packed along [001] direction. The manganese atom (Mn1) is octahedrally coordinated to four coplanar N atoms, while the axial positions are occupied by two O atoms belonging to water molecules. The coordination entities crystallize as shown in Figure 2, where each porphyrinic unit is surrounded by another four, producing an H-bonded 2D supramolecular layer on the xy plane. The robust intralayer H-bonding system is generated by axial water molecules and adjacent porphyrin carboxylate group (2.03 Å) maintaining the stability of the 2D supramolecular array (Table S1, Supplementary Information†). Those 2D layers are stacked along the [001] direction, sustained by a hydrogen bonding system involving the interporphyrin non-localized solvent molecules. During the crystal structure refinement process we have only located one ethanol disordered solvent molecule that is displayed in the voids generated between metalloporphyrinic units.

As mentioned in the introduction section, bta does not result to be coordinated to the metal ion. Even if is not common to mention the fact that the synthesis process does not produce the desirable compounds, in our opinion, this is important as it can be helpful to understand the whole process. In fact, we have already reported [9c] on some syntheses where one of the ligands has not been incorporated to the solid network but they play some significant roles (as crystallisation molecules or modulating agents [9e]).
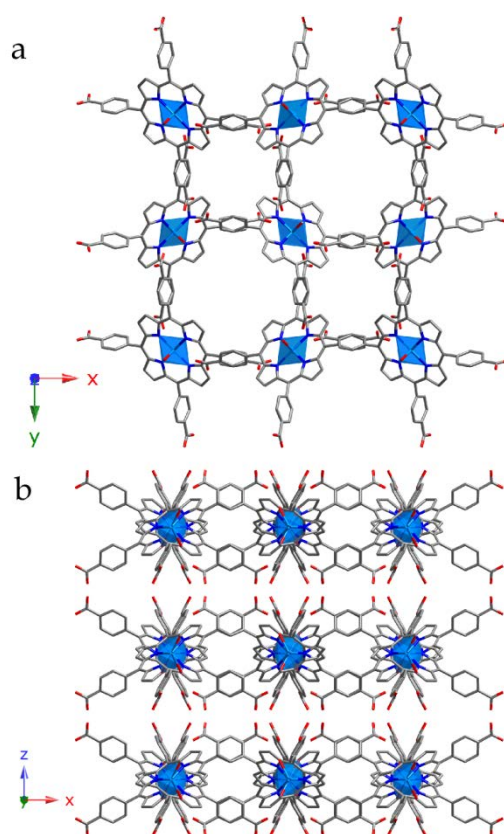
Figure 2. (a) H-bonded 2D supramolecular layer and (b) packing of these layers for compound **2**. (Mn: blue, C: grey, N: dark blue, O: red). H atoms have been omitted for clarity.

3.2. Thermal analysis

In order to know more about the thermal behaviour and stability of compound **1**, thermal characterization was carried out using thermogravimetric and thermodiffractometric experiments. A powdered sample was used, taken immediately after synthesis.

3.2.1. Thermogravimetric analysis

The thermogravimetric decomposition curve shows a two-stage mass loss. First step occurs between 25-100 °C with 14.5% weight loss (attributed to solvent molecules). The second one from 340 °C to 500 °C with 56.8% weight loss, has been attributed to the calcinations of the TCPP units (Figure 3). The residue (27.9%) has been identified by X-ray powder diffraction as Mn_2O_3 [S. G. Fd-3m, a = 8.11 Å][14].
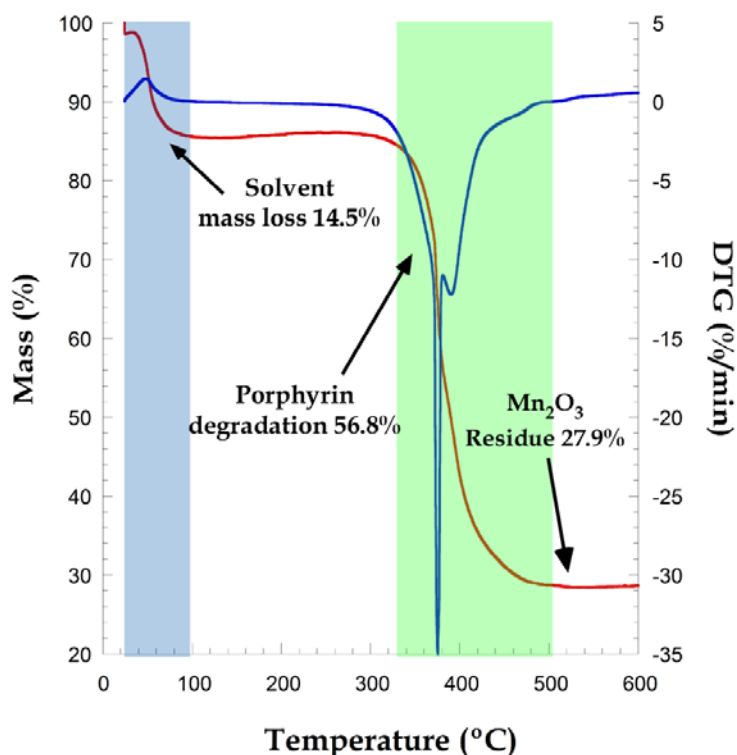
Figure 3. Thermogravimetry for compound **1**.

3.2.2. Thermodiffractometric analysis

The X-ray thermodiffractometry (XRTD) shows that thermal stability of compound **1** is remarkably high. In fact, XRTD analysis reveals that it remains stable up to 360 °C (Figure 4). Above this temperature Mn_2O_3 residue is formed. This high stability can be attributed to the robust layered structure and the hydrogen bonding between layers.
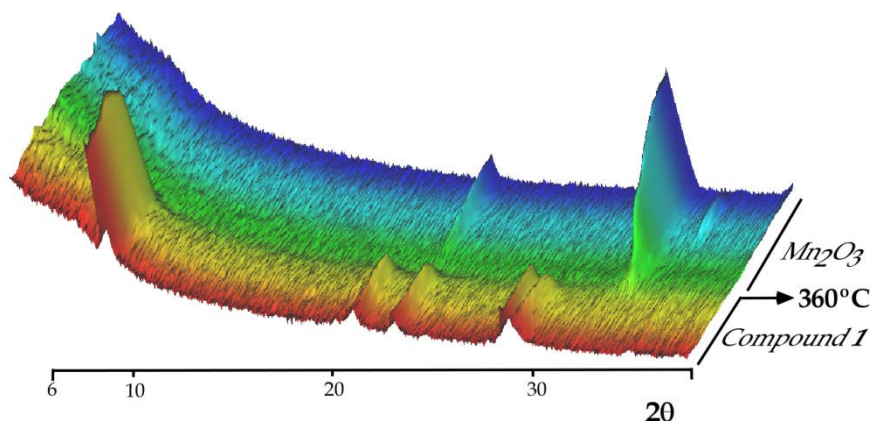

Figure 4. X-ray thermodiffractogram for compound **1**.

3.3. Electron Paramagnetic Resonance (EPR)

X-band EPR spectroscopy has been carried out at room temperature for the sample 3 days after the synthesis (Figure 5). Making a Lorentz adjustment for layered compound **1**, the spectrum shows a signal with the g-tensor value at $g = 2.01$. In spite of the fact that the adjustment confirms the presence of Mn^{II}, it doesn't fit perfectly with the structural model of compound 1 (R=0.99900), suggesting that a second contribution is given. In fact, adjustment improves when is fitted to two contributions (R=0.99987)

with the same g value and a higher width of line. Attempts to adjust the spectrum with other contributions was not satisfactory.

This fact indicated that the second phase also contained Mn^{II}. The low contribution of the second phase could have led to think of it as an impurity. (Figure S4, Supplementary Information†).

This second minor phase was not previously detected on freshly synthesized samples. So, the presence of a new phase on samples kept in mother liquor after several days indicated the occurrence of some kind of transformation. Therefore we proceeded to study this process.
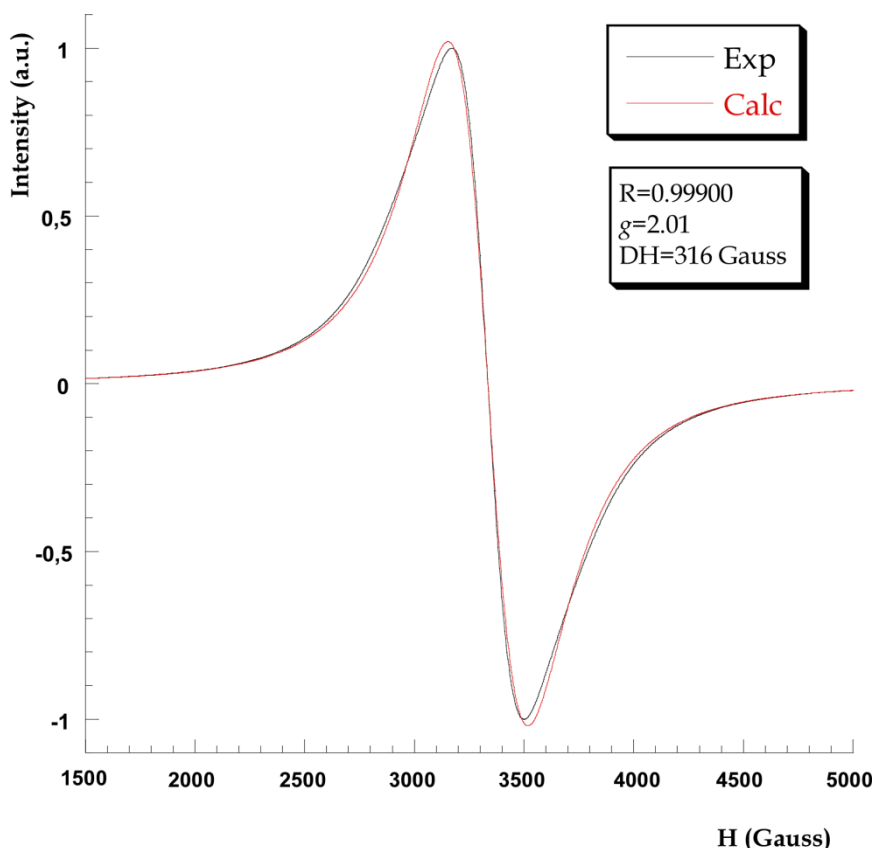

Figure 5. X-Band EPR and adjustment using structural model of compound **1**. (DH= width of line)

3.4. Solid-state transformation analysis

An X-ray diffraction analysis of powdered sample was carried out immediately after synthesis, under conditions specified in experimental section. The refinement was realized in C2/m space group, using cell parameters obtained from structural solution and refinement of compound **1**, by means of FULLPROF SUITE[15]. Refinement option of the complete diagram profile without structural model was used (Pattern Matching), refining cell parameters, the axis displacement, the peak shape, the full width at half maximum (U, V, W) and the asymmetry of the peaks (Figure S5, Supplementary Information†). A value of χ2 of 2.78 was achieved, confirming that the major phase after synthesis is compound **1**.

Besides, several experimental X-ray patterns at different times were carried out with the aim of checking the evolution of both phases with time (Figure S6, Supplementary Information†).

Three one-hour diffractograms were carried out along the time, from 6 to 17 in 2θ (range in which the most intense peaks of each phase appear), with the sample removed from mother-liquor, washed several times with ethanol and keeping it in single crystals. First X-ray diagram was taken several minutes after synthesis; the second one, after 5 days; and the third one, after 15 days. After each measurement, the sample was reintroduced in the mother liquid. As shown in Figure S6, a widening of the peak at 11.5° in 2θ occurs (corresponding to characteristic peak of compound **1**). Additionally, the appearance of the new peak at 8.3°, corresponding to characteristic maximum of compound **2** is observed. This suggests that the monoclinic phase (**1**) gradually transforms into the tetragonal one (**2**), until both phases coexist.

In order to determine if **1** may transform completely into **2** after sufficient time, several X-ray patterns were taken after 15 days. The diagrams remain without changes. Besides, single crystals (taken after one month) have been measured by single crystal X-ray diffraction, confirming the presence of both compounds. Therefore, complete transformation of **1** into **2** has been discarded.

As said before, aspects related to the solid-state transformations can be studied through distortion features (affecting both the coordination sphere and the tetrapyrrolic macrocycle) and DFT calculations.

3.4.1. Distortion of polyhedra

Distortion of coordination polyhedra has been evaluated according to Avnir et al.[16] method, based on the continuous symmetry measures (CSM), by means of SHAPE program,[17] and the results can be seen on Table 2 and Table 3.

Table 2. Distortion values calculated for the hexacoordinated spheres of compounds **1** and **2** (calculated by means of SHAPE software).

	Hexacoordinate	$S(O_h)$	$S(D_{3h})$
Compound **1**	Mn(2)	2.64	18.40
Compound **2**	Mn(1)	0.32	16.74

Table 3. Distortion values calculated for the pentacoordinated spheres of Mn (1) of compound **1** (calculated by means of SHAPE software).

	Pentacoordinated	$S(D_{3h})$	$S(C_{4v})$
Compound **1**	Mn(1)	0.180	5.466

The projection of the as-calculated values on the distortion diagram[18] can be seen in Figure S7, Supplementary Information†. As observed, for compound **1**, results indicate that there is a Jahn-Teller distortion for octahedral Mn(2), in fact the axial Mn(2)–O0AA distance is longer than equatorial ones, and the cis and trans N-Mn(2)-N angles go from 89.5(2)° to 90.5(2)°, and 180°, respectively. Distortion analysis for

Mn(1), in the paddle-wheels, shows a little Berry-type distortion, near to an ideal square pyramid shape. Bond distances and angles are reported in Table S2, Supplementary Information†.

Distortion of coordination polyhedra was also evaluated for compound **2** and results indicate that Mn(1) octahedra are nearly ideal. In fact, the metal atom lies on a four-fold inversion centre, and therefore Mn(1)–N distances have two related values (2.015(4) Å and 2.011(5) Å). On the other hand, cis and trans angles for Mn(1) go from 89.99(10) to 90° and for 179.99(10)° to 180.0°, respectively (Table S2, Supplementary Information†).

These results are consistent with the coordination sphere trying to achieve the ideal octahedral coordination.

3.4.2. Distortion of porphyrins

Distortion of macrocycles has been also analyzed for compounds **1** and **2**. There are six types of distortion defined for non-planar porphyrins: saddle (sad), ruffle (ruf), dome (dom), wavy(x) (wav(x)), wavy(y) (wav(y)) and propeller (pro). The out-of-plane distortion of the porphyrin macrocycles was analyzed by the normal-coordinate structural decomposition method developed by Shelnutt et al. (NSD).[19]

Macrocycles for compounds **1** and **2** show a similar deformation. In fact both are slightly wavy distorted planes. Whereas for compound **1** the total out of plane displacement of the porphyrinic plane (0.1044) is equally distributed between wavy(x) (wav(x)) (49.7%) and wavy(y) (wav(y)) (49.9%), compound **2** is much flatter (0.0281) and just affected by the wavy(y) (wav(y)) type of distortion (96.8%).

As shown in Figure 6 the porphyrin macrocycle in **1** shows the two opposing pyrrole rings tilted up and down with respect to the porphyrin mean plane, while for **2** just two opposing rings are tilted up and down, remaining the other two on the mean plane which indicates the wavy(y) type of distortion.
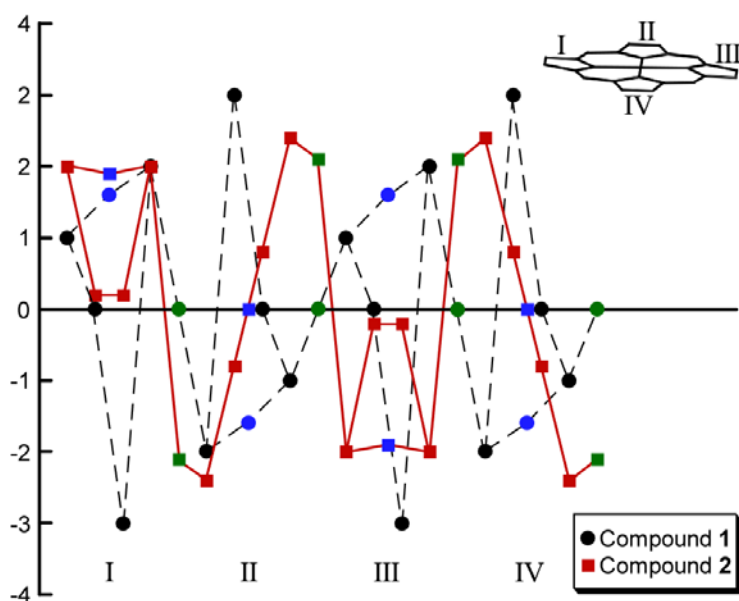
Figure 6. Out-of-plane displacements (in units of 0.01 Å) of the porphyrin core atoms from the mean porphyrin plane (of 24 atoms). Pyrrolic nitrogen atoms are marked in blue and meso carbon atoms in green.

Although the total distortion of both macrocycles is small, it is clear that the porphyrin core in **2** is much more perfect with less deviation of the atoms from the mean plane. This may suggest that the formation of compound **2** is favored to accommodate a porphyrin core exhibiting less stress.

3.4.3. DFT calculations

DFT calculations were also carried out on representative structural fragments of compounds **1** and **2** (Figure S8, Supplementary Information†) which were analyzed by means of quantum-mechanical DFT calculations (Gaussian 03 program).[20] In order to compare calculated values, Mn(1) atoms were removed from compound **1**. DFT single point energy calculations were performed using Becke's three-parameter hybrid functional with the correlation functional of Lee, Yang, and Parr (B3LYP)[21] including the D3 version of Grimme's dispersion.[22] The lanl2DZ basis set was used for Mn and 3-21G for the rest of the atoms, as implemented in Gaussian 09 Rev D01. The convergence of the calculations was not very tight but it was enough to show that the energy of fragment for compound **1** (-11609.6875 Hartrees) is lower than the corresponding one for **2** (-11609.2551 Hartrees).

In this way, DFT calculations support the idea that compound **2** is more stable than compound **1**, which is consistent with the fact that distortion for compound **2** is lower, giving further coherence to the observed transformation.

3.4.4. Cationic Mn^{2+}/H^+ exchange

Taking into consideration the above mentioned aspects, we can propose the following hypothesis for the **1**→**2** transformation. In our opinion, there is a spatial rearrangement of the tetrapyrrolic units as a consequence of the removal of Mn^{2+} ions from paddle-wheels in compound **1** (Figure 7). For this to occur, the equilibrium $[Mn_3(TCPP)]+4H^+ \leftrightarrow [Mn(H_4TCPP)]+2Mn^{2+}$ is established where the charge transference through the cationic exchange involves Mn^{II} atoms.

There are some possible sources of H^+ ions in the synthesis medium: H_2O, DMF and bta. Due to solvothermal conditions, we cannot establish the proton origin just by using concepts like acidity.
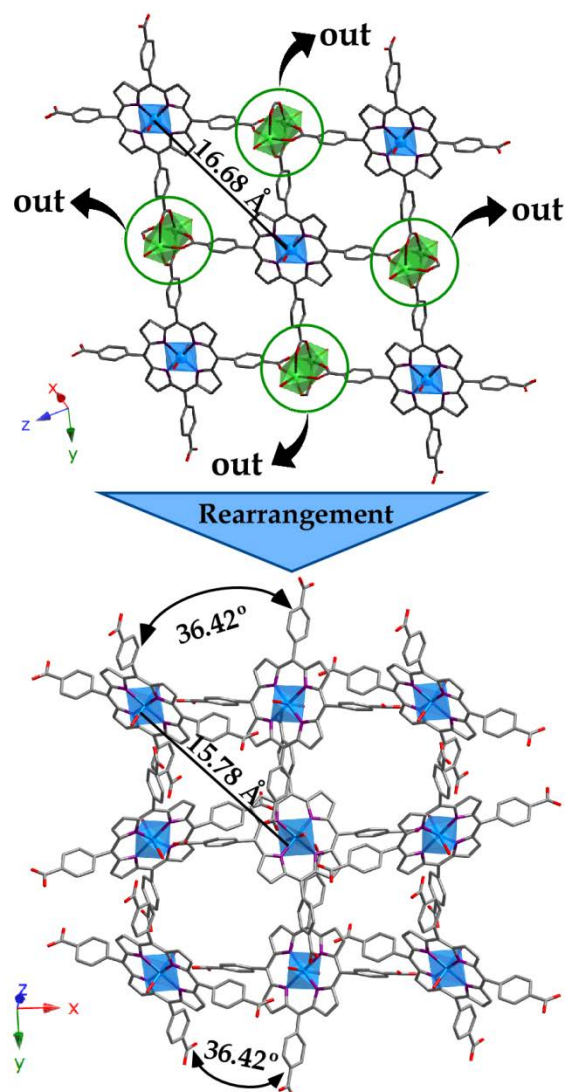
Figure 7. Rearrangement of the crystal structure from compound **1** to compound **2** as a consequence of the crystal-to-crystal transformation.

4. Conclusions

A novel MnII-TCPP compound (**1**) has been obtained by hydrothermal synthesis which undergoes a low-rate, low-speed transformation into a second phase (**2**), when crystals are kept in mother liquor.

Solid-state transformations in MOFs usually involve exchange of guest molecules, so the transformation herein studied is quite unusual because it involves a cationic exchange between two solid phases that are in the mother liqueur. This exchange takes place in ambient conditions (20 °C, 1 atm), and it was detected by means of EPR measurements which are extremely sensitive to variations in the coordination sphere of metal ions.

Acknowledgements

References

[1] K. M. Kadish, K. M. Smith, R. Guilard, The Porphyrin Handbook, Academic Press, San Diego, 2000-2003.

[2] W. Y. Gao, M. Chrzanowski, S. Ma, Chem. Soc. Rev. 43 (2014) 5841-5866; b) T. F. Liu, D. Feng, Y. P. Chen, L. Zou, M. Bosch, S. Yuan, Z. Wei, S. Fordham, K. Wang, H. C. Zhou, J. Am. Chem. Soc. 137(1) (2015) 413-419; c) T. Rhauderwiek, S. Waitschat, S. Wuttke, H. Reinsch, T. Bein, N. Stock, Inorg. Chem. 55(11) (2016) 5312–5319.

[3] a) I. Beletskaya, V. S. Tyurin, A. Y. Tsivadza, R. Guilard, C. Stern, Chem. Rev. 109 (2009) 1659-1713; b) C. M. Drain, A. Varotto, I. Radivojevic, Chem. Rev. 109 (2009) 1630-1658; c) I. Goldberg, CrystEngComm 10 (2008), 637-645.

[4] a) J. R. Long, O. M. Yaghi, Chem. Soc. Rev. 38 (2009) 1213-1214; b) L. R. MacGillivray, Metal-Organic Frameworks: Design and Application Wiley, 1 edn 2010; c) H.-C. Zhou, J. R. Long, O. M. Yaghi, Chem. Rev. 112 (2012) 673-674; d) K. K. Tanabe, S. M. Cohen, Chem. Soc. Rev. 40 (2011) 498-519; e) O. K. Farha, J. T. Hupp, Acc. Chem. Res. 43 (2010) 1166-1175.

[5] A. Calderón-Casado, G. Barandika, B. Bazan, M. K. Urtiaga, O. Vallcorba, J. Rius, C. Miravittles, M. I. Arriortua, CrystEngComm 13 (2011) 6831–6838.

[6] a) J. Canivet, A. Fateeva, Y. Guo, B. Coasne, D. Farrusseng, Chem. Soc. Rev. 43 (2014) 5594-5617; b) S. Han, Y. Huang, T. Watanabe, S. Nair, K. S. Walton, D. S. Sholl, J. C. Meredith, Micropor. Mesopor. Mater. (2013) 173, 86–91; c) S. Zuluaga, E. M. Fuentes-Fernández, K. Tan, F. Xu, J. Li, Y. J. Chabal, T. Thonhauser, J. Mater. Chem. A 4 (2016) 5176-5183; d) K. Tan, N. Nijem, P. Canepa, Q. Gong, J. Li, T. Thonhauser, Y. J. Chabal, Chem. Mater. 24 (2012) 3153−3167.

[7] a) S. Kitagawa, K. Uemera, Chem. Soc. Rev. 34 (2005) 109-119; b) L. J. Barbour, Aust. J. Chem. 59 (2006) 595-596; c) J. Seo, R. Matsuda, H. Sakamoto, C. Bonneau, S. Kitagawa, J. Am. Chem. Soc. 131 (2009) 12792-12800; d) A. M. Chippindale, S. J. Hibble, J. Am. Chem. Soc. 131 (2009) 12736-12744; e) D.-X. Xue, W.-X. Zhang, X.-M. Chen, H.-Z. Wang, Chem. Commun. 44 (2008) 1551-1553. f) J. J. Vittal, Coord. Chem. Rev. 251 (2007) 1781-1795.

[8] M. H. Mir, L. L. Koh, G. K. Tan, J. J. Vittal, Angew. Chem. Int. Ed. 49 (2010) 390–393.

[9] a) A. Fidalgo-Marijuan, E. Amayuelas, G. Barandika, B. Bazan, M. K. Urtiaga, M. I. Arriortua, Molecules 20 (2015) 6683-6699; b) A. Fidalgo-Marijuan, G. Barandika, B. Bazan, M. K. Urtiaga, M. I. Arriortua, CrystEngComm 15 (2013) 4181-4188; c) L. Bravo-García, G. Barandika, B. Bazan, M. K. Urtiaga, M. I. Arriortua, Polyhedron 92 (2015) 117–123; d) A. Fidalgo-Marijuan, G. Barandika, B. Bazan, M. K. Urtiaga, M. I. Arriortua, Polyhedron 30 (2011) 2711–2716; e) E. Amayuelas, A. Fidalgo-Marijuan, G. Barandika, B. Bazan, M. K. Urtiaga, M. I. Arriortua, CrystEngComm 17 (2015) 3297-3304.

[10] W. Yinghua, J. Appl. Crystallogr. 20 (1987) 258-259.

[11] CrysAlisPro Software System Agilent Technologies UK Ltd., Oxford, Uk, 2012.

[12] O. V. Dolomanov, L. J. Bourhis, R. J. Gildea, J. A. K. Howard, H. Puschmann, J. Appl. Crystallogr. 42 (2009) 339-341.

[13] G. M. Sheldrick, Acta Crystallogr., Sect. A: Found. Crystallogr. A64 (2008) 112-122.

[14] Powder Diffraction File-Inorganic and Organic, ICCD, File: 00-041-1442. Pensylvania, USA 2001.

[15] (a) J. Rodríguez-Carvajal, Recent Developments of the Program FULLPROF, in Commission on Powder Diffraction (IUCr) Newsletter 26 (2001) 12-19; (b) J. Rodríguez-Carvajal J., FULLPROF SUITE Program. Rietveld Pattern Matching Analysis of Powder Patterns, 1994.

[16] a) H. Zabrodsky, S. Peleg, D. Avnir, J. Am. Chem. Soc. 114 (1992) 7843-7851; b) M. Pinsky, D. Avnir, Inorg. Chem. 37 (1998) 5575-5582.

[17] M. Llunel, D. Casanova, J. Cirera, J. M. Bofill, P. Alemany, S. Álvarez, M. Pinsky, D. Yatunir, SHAPE v1.1a, "Program for Continuous Shape Measure Calculations of Polyhedral Xn and MLn Fragments" 2003.

[18] S. Álvarez, P. Alemany, D. Casanova, J. Cirera, M. Llunell, D. Avnir, Coord. Chem. Rev. 249 (2005) 1693-1708.

[19] a) W. Jentzen, J. -G. Ma, J. A. Shelnutt, Biophys. J. 74 (1998) 753-763; b) W. Jentzen, X. -Z. Song, J. A. Shelnutt, J. Phys. Chem. B 101 (1997) 1684-1699; http://bit.ly/20PvBm0

[20] M. J. Frisch, G. W. Trucks, H. B. Schlegel, G. E. Scuseria, M. A. Robb, J. R. Cheeseman, J. A. Montgomery, J. Vreven, T., K. N. Kudin, J. C. Burant, J. M. Millam, S. S. Iyengar, J. Tomasi, V. Barone, B. Mennucci, M. Cossi, G. Scalmani, N. Rega, G. A. Petersson, H. Nakatsuji, M. Hada, M. Ehara, K. Toyota, R. Fukuda, J. Hasegawa, M. Ishida, T. Nakajima, Y. Honda, O. Kitao, H. Nakai, M. Klene, X. Li, J. E. Knox, H. P. Hratchian, J. B. Cross, V. Bakken, C. Adamo, J. Jaramillo, R. Gomperts, R. E. Stratmann, O. Yazyev, A. J. Austin, R. Cammi, C. Pomelli, J. W. Ochterski, P. Y. Ayala, K. Morokuma, G. A. Voth, P. Salvador, J. J. Dannenberg, V. G. Zakrzewski, S. Dapprich, A. D. Daniels, M. C. Strain, O. Farkas, D. K. Malick, A. D. Rabuck, K. Raghavachari, J. B. Foresman, J. V. Ortiz, Q. Cui, A. G. Baboul, S. Clifford, J. Cioslowski, B. B. Stefanov, G. Liu, A. Liashenko, P. Piskorz, I. Komaromi, R. L. Martin, D. J. Fox, T. Keith, M. A. Al-Laham, C. Y. Peng, A. Nanayakkara, M. Challacombe, P. M. W. Gill, B. Johnson, W. Chen, M. W. Wong, C. Gonzalez, J. A. Pople, GAUSSIAN 03, (Revision D.02), Gaussian, Inc., Wallingford CT, 2004.

[21] a) A. D. Becke, J. Chem. Phys. 98 (1993) 5648-5652; b) C. Lee, W. Yang, R. G. Parr, Phys. Rev. B: Condens. Matter 37 (1988) 785-789.

[22] S. Grimme, J. Antony, S. Ehrlich, H. Krieg, J. Chem. Phys. 132 (2010) 154104-154119.